Journal of Applied Polymer Science

Performance and mechanism of laser transmission joining between glass fiber-reinforced PA66 and PC

Huixia Liu,[1] Guochun Chen,[1] Hairong Jiang,[1] Dehui Guo,[1] Zhang Yan,[1] Xuelian Wu,[1] Pin Li,[2] Xiao Wang[1]

[1]School of Mechanical Engineering, Jiangsu University, Zhenjiang, 212000, People's Republic of China
[2]School of Mechanical Engineering, Shanghai Jiao Tong University, Shanghai, 200000, People's Republic of China
Correspondence to: H. Liu (E-mail: lhx@ujs.edu.cn)

ABSTRACT: On account of the large compatibility difference between glass fiber-reinforced Polyamide 66 (GFR-PA66) and Polycarbonate (PC), it is difficult to weld them directly by laser. A new technology is introduced in this article by which the transparent PC is successfully welded with GFR-PA66 using cold spraying in order to spray a 20 μm-thick aluminum film on GFR-PA66 as the absorbed layer. Tensile shear tests show the tensile strength of welded joints is highly enhanced. The influences of bubbles, glass fiber, and aluminum atoms on the performance of the joins are investigated via the optical microscope. X-ray Photoelectron Spectrometer (XPS) is used to detect the chemical information of fracture sections on PC. In terms of the generation of bubbles, the influence of glass fiber, the distribution of aluminum atoms, and the formation of new chemical bonds, this article analyses the mechanism why the two different materials can be welded successfully. The micro-anchor influence of glass giber in fiber-reinforced polymers is important. The generation of new chemical bonding (Al–O–C) between aluminum and upper PC is the main reason why the joining strength is enhanced greatly. © 2015 Wiley Periodicals, Inc. J. Appl. Polym. Sci. **2016**, *133*, 43068.

KEYWORDS: coatings; microscopy; polyamides; thermoplastics; X-ray

Received 6 July 2015; accepted 16 October 2015
DOI: 10.1002/app.43068

INTRODUCTION

In recent 30 years, micro electro mechanical systems (MEMS) have gained great progress. As for highly precise MEMS, silicon is commonly used. However, with the application areas more and more widely, silicon cannot satisfy the vast demands alone.[1] Compared with other materials, polymers have many advantages, such as low production cost, high optical transparency, and easy to fabrication. What's more, polymers can fit in many different occasions where different mechanical strength and surface chemical activity are needed.[2,3] For example, microfluidic devices, implantable electronic devices, micro sensors, and so on.

However, in practical industrial production, the realization of real products can be achieved only by the optimal integration of different materials and the proper joining technology. So, the connection of different kinds of polymers in MEMS is also very important.

Sunkara *et al.*[4] successfully joined the thermoplastic polycarbonate (PC), cycloolefin copolymer (COC), polymethyl methacrylate (PMMA), and polystyrene (PS) with elastomeric polydimethylsiloxane (PDMS) to fabricate micro fluidic components via chemical modification. The tensile strength of composite components after connection can reach 430, 432, 385, and 388 kPa, respectively, among PC/PDMS, COC/PDMS, PMMA/PDMS, and PS/PDMS. Qin *et al.*[5] used polymers for encapsulation of different micro elements, such as microelectrode units, remote sensing coil, structural membrane, and implantable sensors for packaging and coating. Jang *et al.*[6] successfully connected two PC sheets through surface chemical modification to make sensor cell-arrays whose tensile strength was 0.55 MPa. Schmidt *et al.*[7] studied the effect of long fiber-reinforced PA composite on laser joining. Jaeschke *et al.*[8] discussed the heat absorption effect of carbon fiber orientation in the laser joining of two same kinds of composites poly phenylene snlfide (PPS). However, the joining strength among different kinds of materials is not very high because of the melting points and compatibility difference. So there has been many researches of the laser transmission joining using same kinds of materials. However, studies about joining different kinds of fiber-reinforced composite polymers which are not compatible are relatively fewer.

PC is a kind of thermoplastics, which contains several reactive functional groups such as the ester groups and benzene rings. Due to its high transparency, excellent mechanical property (young modulus: 2.0–2.4 GPa), high glass transition temperature

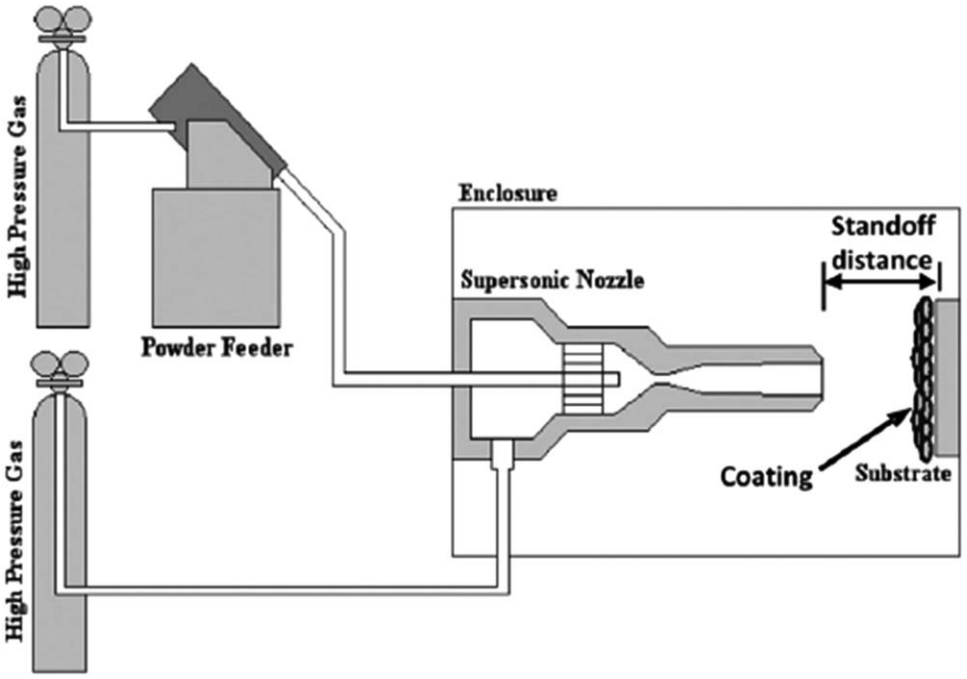

Figure 1. The schematic diagram of the cold spraying set-up.

(145°C), and good biocompatibility, PC is widely applied in MEMS, especially in micro fluidic components.[6] As for glass fiber-reinforced Polyamide 66 (GFR-PA66), it has high specific strength, good fatigue resistance, excellent vibration reduction performance, high temperature resistance, and easy for processing (low elasticity modulus). So, it is a promising kind of polymers in MEMS.

Generally, amino exchange reaction is apt to occur when PC and PA66 are in fusion conditions resulting in decrease of molecular weight. The internal carbonate groups of PC may react with the amino terminal groups of PA6 during the melt mixing process at 240°C.[9] That is the very reason why they are difficult to be welded by laser.

In this study, to solve this problem, a 20 μm-thick aluminum film was sprayed on the surface of GFR-PA66 via the cold spraying technology as a buffer and transition layer to improve the welding compatibility. In order to evaluate the joining performance of the laser lap joints, tensile shear tests were conducted. The fracture morphology, cross-sectional morphology, and the distribution of aluminum atoms were observed by optical microscope. Furthermore, the chemical information was examined with X-ray Photoelectron Spectrometer (XPS) to ensure whether there were new chemical bonds or not. Above all, the mechanism of laser transmission joining between pretreated GFR-PA66 and PC was explained in detail.

EXPERIMENTAL

Cold Spraying

Under the process of cold spraying, metal powders are accelerated by high pressure carried gas so as to hit on the substrate through the trumpet nozzle, which has a big inlet and a small outlet. The deformation of particles in powders occur due to high kinetic energy, so they can generate effective bonding and form a homogeneous metal layer.[10] Compared with traditional metallization methods of polymer surfaces, the heat generated in the process of cold spaying is relatively less. The thermal effects can be reduced a lot, such as thermal surface deformation, oxidation, voids in degradation, crystalline phase transition, and so on.[10–13] The schematic diagram of the cold spraying set-up is shown in Figure 1.

Materials

GFR-PA66 sheets with 20% volume of glass fiber were used in the experiments with dimensions of 50 mm×20 mm×2 mm, and the dimensions of PC sheets were 50 mm×20 mm×0.8 mm. (The master batch type is 101F, DuPont Engineering Polymers. The sheets were produced by injection molding.) All samples were cleaned by the ultrasonic cleaning machine, and placed in a drying oven about 12 h before experiments.

Then the GFR-PA66 sheets were cold sprayed under room temperature. Through cold spaying technology, a 20 μm-thick aluminum membrane was sprayed on the surface of GFR-PA66. (The metal powders were produced by OPSC, Russia.) In Figure 2, the micrograph of GFR-PA66 surface after cold spayed is shown.

Laser Transmission Joining

The laser transmission joining processes were conducted with the Copmact130/140 semiconductor continuous laser machine manufactured by DILAS. The maximum power of the laser device is 130 W, the wavelength of laser is 980 ± 10 nm, and the minimum beam diameter is 700–800 μm. The whole system works at the temperature between 15°C and 25°C, and the scope of speed is 0∼3000 mm/min. In this study, the laser power of 25 W, the welding speed of 300 mm/min, and the laser spot

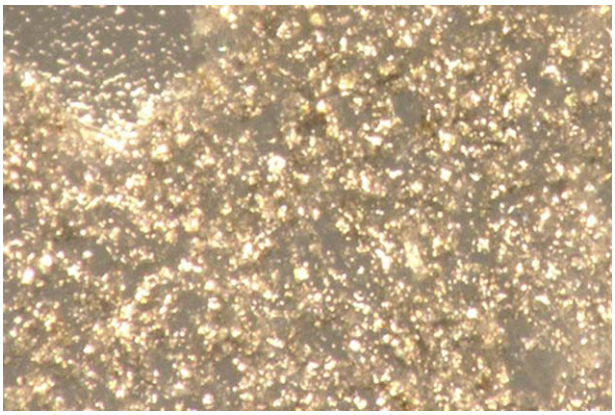

Figure 2. The micrograph of GFR-PA66 surface after cold spayed. [Color figure can be viewed in the online issue, which is available at wileyonlinelibrary.com.]

diameter of 2 mm were used. The schematic diagram of laser transmission joining GFR-PA66/PC is shown in Figure 3.

Tensile Shear Tests

After laser welding, the tensile shear tests of the joining lap joints were performed by the universal tensile machine at a tensile speed of 2 mm/min under room temperature. Through microcomputer control system, it can realize the uploading of tensile strength in a constant speed. The loading force and amount of deformation are displayed on the monitor. The calculation equation of the tensile strength is as the eq. (3-1) shows:

$$\sigma_t = F / (b \times d) \qquad (3\text{-}1)$$

where σ_t is the tensile strength (MPa), F is the maximal tensile force (N), b represents the weld seam length (mm), and d represents the weld seam width (mm). The schematic diagram of tensile shear tests is shown in Figure 4.

Observation of Microstructure and Analysis of Chemical Information

Cutting out metallographic specimens along the cross sections of the lap joints, the fracture morphology, and cross-sectional

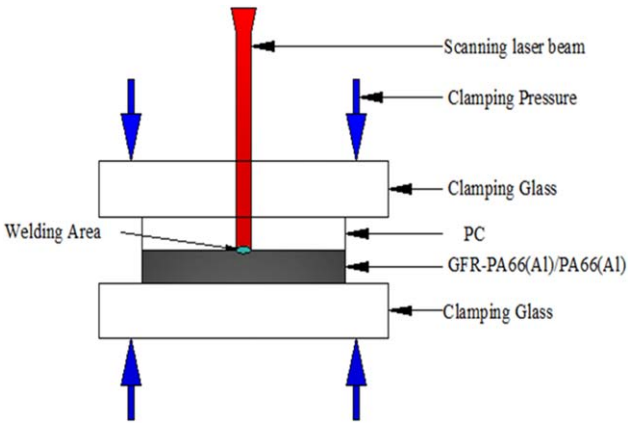

Figure 3. The schematic diagram of laser transmission welding GFR-PA66/PC. [Color figure can be viewed in the online issue, which is available at wileyonlinelibrary.com.]

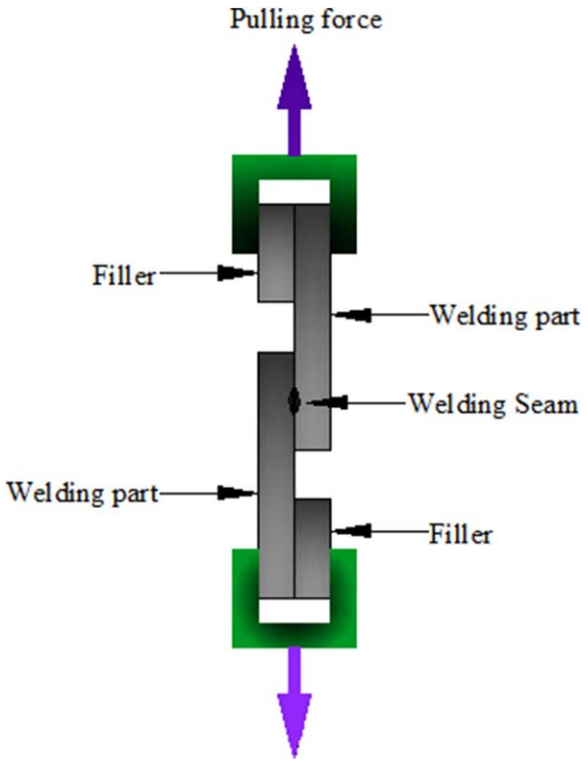

Figure 4. The schematic diagram of tensile shear tests. [Color figure can be viewed in the online issue, which is available at wileyonlinelibrary.com.]

morphology can be observed with the true color confocal 3D microscope.

To examine whether aluminum atoms react with PC resulting in new chemical bonds or not, X-ray Photoelectron Spectrometer (XPS) is used to detect the chemical information of fracture sections on PC.

RESULTS AND DISCUSSION

Influences of Bubbles on the Performance of Joints

As is shown in Figure 5, there are many tiny and evenly distributed bubbles around the weld seam on PC sheets. During the laser joining process, there is much heat generated resulting in the degradation of PC. So, there are many bubbles. These bubbles mainly consist of water vapor, carbon dioxide, carbon monoxide, and hydrocarbons.[14] The high pressure generated by these tiny homogeneous bubbles can force upper fused PC to the pits and cracks on the surface of GFR-PA66 sheets. Thus, the two materials can realize micro-anchor mechanism and increase the joining strength.

Liu *et al.*[15] studied joining of aluminum alloy to polyethylene glycol terephthalate (PET) using friction lap welding. They also discovered that these bubbles generate high pressure pushing the fused polymers to the pits and micro voids on the surface of metal, which can supply more mechanical bonding and realize tight joining between metal and polymers. Katayama *et al.*[16] also found that evenly distributed bubbles were beneficial to improve the joining strength.

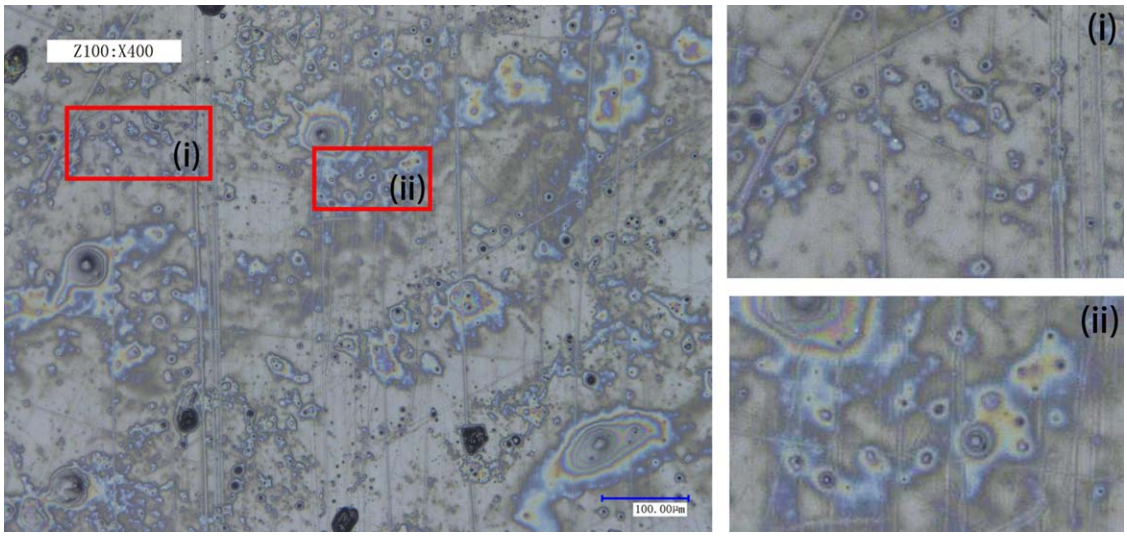

Figure 5. Micrograph of the welding seam on PC side and partial enlarged graphs. [Color figure can be viewed in the online issue, which is available at wileyonlinelibrary.com.]

Effects of Glass Fiber on Joining Strength

The micrograph of welding seam on GFR-PA66 side is shown in Figure 6. Aluminum atoms sprayed on the surface of GFR-PA66 can absorb the laser energy directly resulting in the degradation and vanishing of the surface material leaving glass fiber uncovered.

In Figure 7, it is found that the exposed glass fiber and PC form micro-anchor effects after laser transmission joining as is mentioned above. So, it can be inferred that the upper fused PC is forced to the uncovered glass fiber in GFR-PA66 under pressure of clamping glass and high pressure bubbles, which generates micro-anchor and micro-friction effect.

In the study of the adhesive-embossing composite joint between metal substrates and glass fiber-reinforced composite materials, it was also found that the adhesion agent is pushed to the exposed glass fiber under pressure of clamping mold.[17] The surface between them realizes micro-dimension anchoring and additional friction effects, as is shown in Figure 8.

In Figure 9, it is also observed that there are plenty of micron-sized pits on PC after laser joining, and some bright silver aluminum atoms are filled in the pits, which also form micro-sized anchor effect to improve the joining strength.

Effects of Distribution of Aluminum Atoms on Joining Strength

In Figure 10, the boundary of two materials is not that obvious after laser welding. There are many silver spots both in PC and GFR-PA66 sheets. It can be inferred that aluminum atoms aggregate into the fused materials from the surface of GFR-PA66 while welding. Due to the structural characters of inorganic particles themselves, the interaction of different polymeric

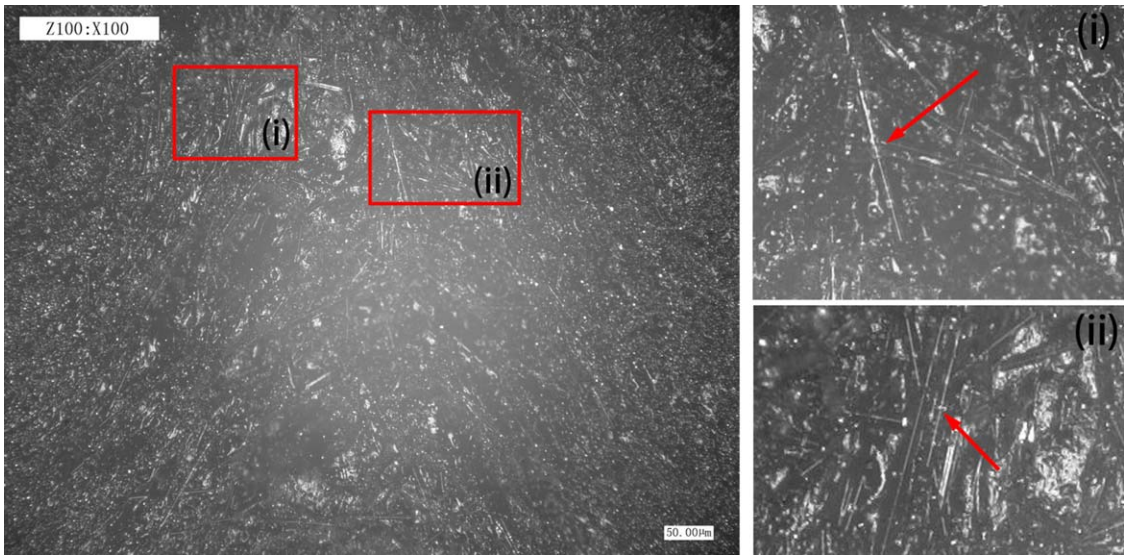

Figure 6. Micrograph of welding seam on GFR-PA66 side and partial enlarged graphs. [Color figure can be viewed in the online issue, which is available at wileyonlinelibrary.com.]

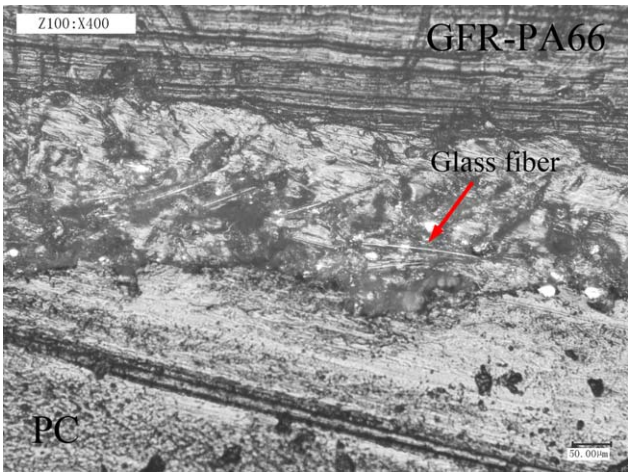

Figure 7. Cross-sectional micrograph of GFR-PA66/PC welding seam. [Color figure can be viewed in the online issue, which is available at wileyonlinelibrary.com.]

components, the viscosity difference, and the attraction effects of molecular chains on particles, and so on, inorganic particles distributed alternatively in different polymeric components.[17]

It is discovered that the smaller the interfacial tension between inorganic particles and polymers is, the better wettability of particles is. In other words, the inorganic particles prefer to distribute in this kind of polymers.[18] The Kono company have announced the surface tension coefficient of some common polymers at 20°C. It shows that the surface tension of PA66 is 46.5 mN/m and the surface tension of PC is 34.2 mN/m.[19] So, the wettability between PC and aluminum atoms is better as for the same kind of inorganic particles and more aluminum atoms can be observed inside PC sheets.

It was also found that the introduced particles can act as compatibilizing agents and help to control the morphological structure of incompatible polymer blends.[20] PA66 and PC are incompatible or partially compatible, so they cannot be welded. The aluminum atoms may improve compatibility of two materials resulting in joining them successfully.

Besides, it is also discovered that in the process of laser transmission joining metal and PET, metal atoms realize atom-level

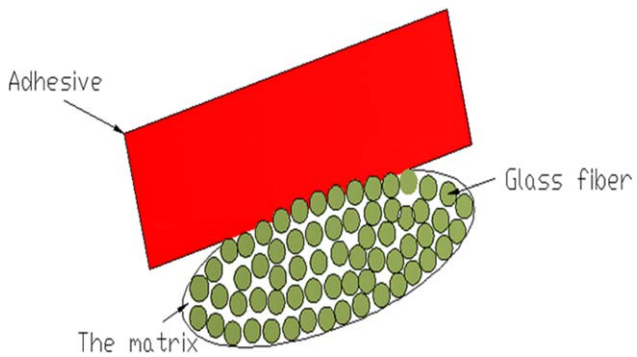

Figure 8. The principle sketch of micro-anchor and micro-friction effect. [Color figure can be viewed in the online issue, which is available at wileyonlinelibrary.com.]

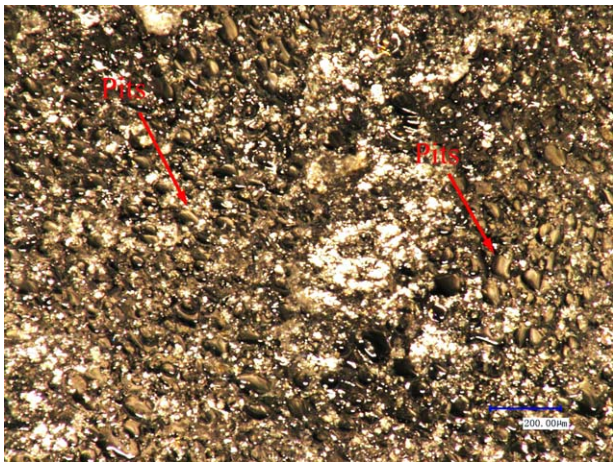

Figure 9. The micrograph of welding joints on PC side. [Color figure can be viewed in the online issue, which is available at wileyonlinelibrary.com.]

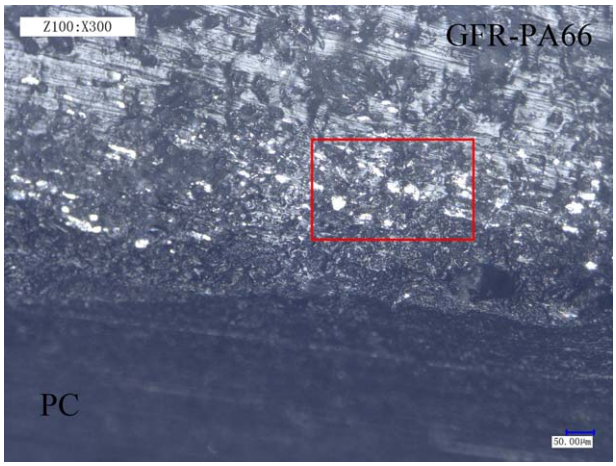

Figure 10. Cross-sectional micrograph of the welding seam. [Color figure can be viewed in the online issue, which is available at wileyonlinelibrary.com.]

or molecule-level connections with polymers. This physical Van der Waals force can improve joining strength a lot.[21,22] It can also supply evidence for welding different kinds of polymers successfully. Above all, it can be inferred that aluminum atoms

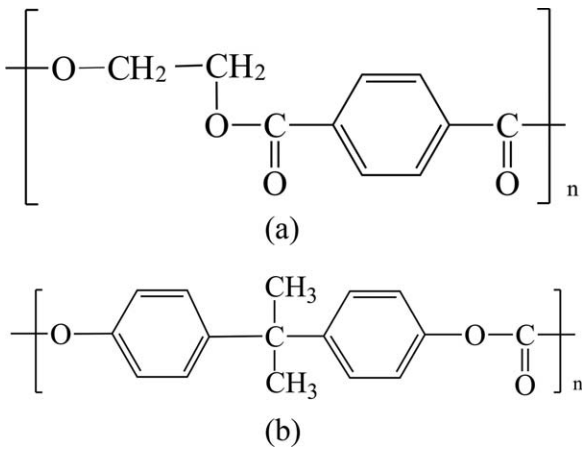

Figure 11. The chemical structural formulas (a) PET and (b) PC.

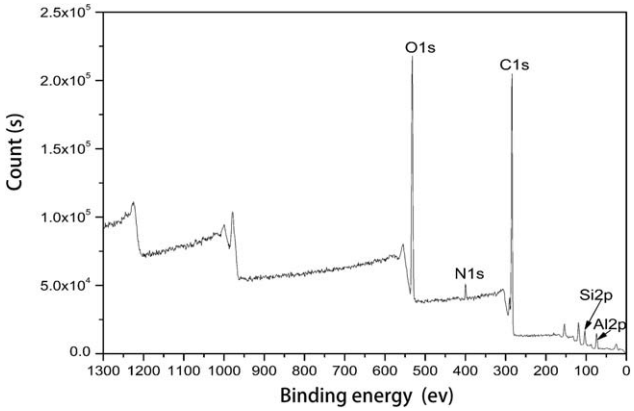

Figure 12. The elements full spectrum diagram of the welding seam on PC side.

and polymer molecular chains draw to each other and form molecular level connection.

X-ray Photoelectron Spectroscopy (XPS)

From the fracture parts of welding joints, it is observed that some aluminum powders and little PA66 adhering to the upper PC. Ali *et al.*[23] studied the joining surface of anodizing alumina film and polyacrylate poly-hydroxyethyl methacrylate (PHEMA), they discovered that the ester groups of PHEMA reacted with aluminum atoms. In the study of alumina films deposited on the surface of corona treated PET, Sandrin *et al.*[24] found that the aluminum atoms reacted with PET and generated new Al–O–C and Al–C chemical bonds.

The chemical structural formulas of PET and PC are shown in Figure 11. They have similar chemical structures both consisting of active functional groups such as benzene rings, ester groups, and so on. It can be inferred that aluminum atoms may react with the upper PC to generate new chemical bonds. So, the XPS is used to perform X-ray photoelectron spectroscopy analysis on the broken surface of PC after tension.

The elements full spectrum diagram of the welding seam on PC side is shown in Figure 12. C, N, O, and Al elements are detected in this area. The existence of N proves that some PA66 adheres to PC. The existence of element Si may be due to the contamination of the clamping devices.

In Figure 13, the C1s peak-differentiation diagrams of pure PC and welded PC are shown.

The binding energy, full width at half-maximum (FWHM), and chemical bonds information corresponding to peaks in C1s graph are summarized in Table I.

The peak whose binding energy is 290.8 eV on the left-most represents the satellite peak. It is used to calculate and compensate the error, which has no effect on the real experimental results.

In the early research, the chemical bond Al–O–C and Al–C kind chemical compound were found at around 283.5 eV and 281.8 eV, respectively.[24] So, it can be inferred that aluminum atoms react with the ester groups in PC, and then generate new chemical bonds (Al–O–C) around 283.6 eV peak. Maybe the amounts of Al–C are relatively less, so it cannot be discovered at around the 282 eV peak.

In Figure 14, there are five peaks. The double peak represents the pure aluminum (the gap between two peaks are 0.4 eV), namely, the two separate peaks at 72.1 eV and 72.5 eV, respectively. It is obviously discovered that the contents of Al_2O_3 are higher than those of pure Al.

The binding energy, full width at half-maximum, and chemical bonds information corresponding to peaks in Al2p graph is summarized in the Table II.

Tang *et al.*[25] studied the chemical reaction between polymer membranes and aluminum. They discovered that Al–O–C was generated at the binding energy of 75 eV. Consequently, based on C1s results above, the rest peak in Al2p represents Al–O–C at 75.5 eV.

In Figure 15, it is discovered that the full width at half-maximum (FWHM) corresponding to C=O becomes wider obviously comparing with that in welded PC peak graph. It is inferred that the new generated Al–O–C is contained in the

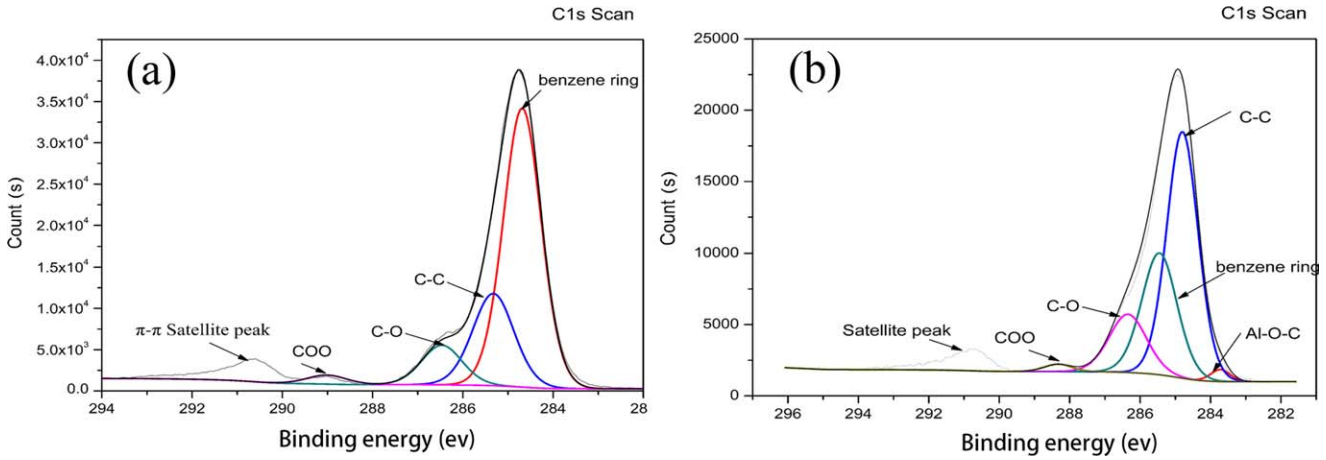

Figure 13. The C1s peak-differentiation diagrams (a) pure PC and (b) welded PC. [Color figure can be viewed in the online issue, which is available at wileyonlinelibrary.com.]

Table I. The Binding Energy, Full Width at Half-Maximum and Chemical Bonds information of Each Peak in C1s Graph

C1s peaks	Binding energy (ev)	FWHM (ev)	Chemical bonds
PC C1s peak	284.7	0.98	benzene ring
	285.3	1.08	C–C
	286.5	1.05	C–O
	289.0	1.02	COO
Welded PC C1s peak			
	283.6	0.65	Al–O–C
	284.7	0.97	Benzene ring
	285.0	1.32	C–C
	286.4	1.25	C–O
	288.3	0.91	COO

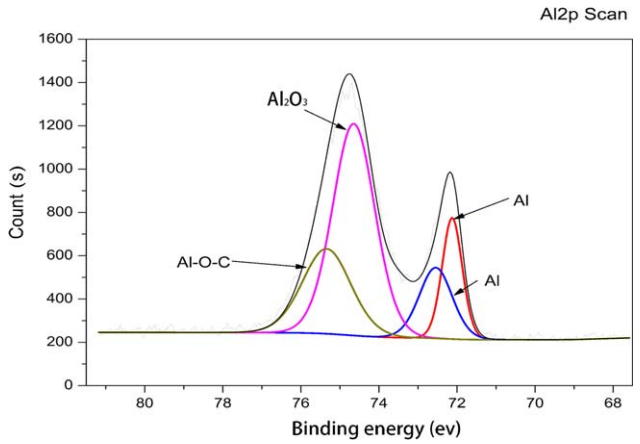

Figure 14. The Al2p peak-differentiation graph of the welding joints on PC side. [Color figure can be viewed in the online issue, which is available at wileyonlinelibrary.com.]

C=O peak. Bébin *et al.*[26] also found this phenomenon in literature.

Tan *et al.*[27] studied effects of Cr plating layer on shear strength and interface bonding characteristics of mild steel/glass fiber reinforced polymers (GFRP) joint by laser heating. They also found that the metal Cr facilitated the opening of C=O groups in polymers resulting in the generation of Cr–O–C compounds. In Ref. 25, it is also observed that Al atoms reacted with benzene rings of PET.

Table II. The Binding Energy, Full Width at Half-Maximum and Chemical Bonds information of Each Peak in Al2p Graph

	Binding energy (ev)	FWHM (ev)	Chemical bonds
Welded PC Al2p peak	72.1	0.6	Al–Al
	72.5	1.0	Al–Al
	74.6	1.27	Al_2O_3
	75.5	1.46	Al–O–C

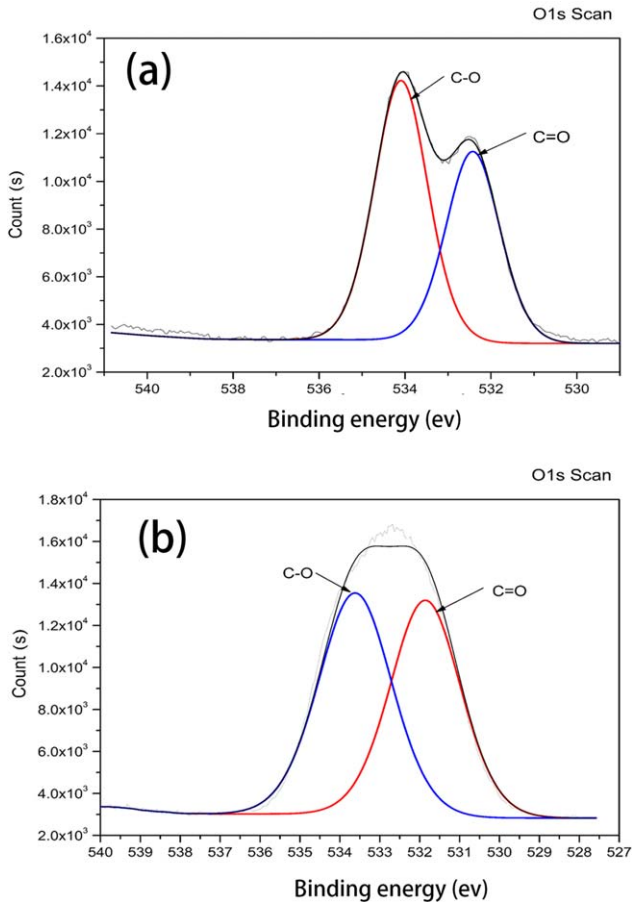

Figure 15. The O1s peak-differentiation diagrams (a) pure PC and (b) welded PC. [Color figure can be viewed in the online issue, which is available at wileyonlinelibrary.com.]

Above all, in the process of laser transmission joining Al atoms sprayed on the surface GFR-PA66 react with the active functional groups (ester groups and benzene rings) of PC and generate Al–O–C chemical bonds improving the tensile strength of joints. However, unsprayed GFR-PA66 failed to be welded with PC, it can be concluded that the chemical bonding between GFR-PA66 and PC is the fundamental reason why they can be laser welded successfully.

CONCLUSIONS

In this article, the transparent PC is successfully welded with GFR-PA66 using cold spraying. Using the new cold spraying technology, GFR-PA66, and PC, which cannot be welded originally, are successfully welded by laser. Furthermore, the joining strength can reach 4 MPa. The generated homogeneous bubbles facilitate the mechanical micro-connection between GFR-PA66 and PC and increase the joining strength. Glass fiber in GFR-PA66 can contribute to the micro-anchor and additional micro-friction between the two materials. It also improves the joining strength. Aluminum atoms can migrate in the fused polymer blends. Served as the connection bridge, aluminum atoms can realize molecular level connection with polymer molecular chains.

Through XPS experiments, aluminum atoms sprayed on the surface GFR-PA66 react with the active functional groups (ester groups and benzene rings) of PC and the generated Al–O–C chemical bonds improve the tensile strength of joints. However, unsprayed GFR-PA66 failed to be welded with PC, it can be concluded that the chemical bonding between Al and PC is the fundamental reason why they can be laser welded.

ACKNOWLEDGMENTS

The authors acknowledge the National Natural Science Foundation of China (Grant No. 51275219) and Key University Science Research Project of Jiangsu Province (14KJB460006).

REFERENCES

1. Zhao, J.; Sheadel, D. A.; Xue, W. *Sens. Actuators A* **2012**, *187*, 43.
2. Liu, C. *Adv. Mater.* **2007**, *19*, 3783.
3. Verpoorte, E.; De Rooij, N. F. *Proc. IEEE* **2003**, *91*, 930.
4. Sunkara, V.; Park, D. K.; Hwang, H.; Chantiwas, R.; Soper, S. A.; Cho, Y. K. *Lab. Chip* **2011**, *11*, 962.
5. Qin, Y.; Howlader, M. R.; Deen, M. J. *Sens. Actuators B* **2014**, *202*, 758.
6. Jang, M.; Park, S.; Lee, N. Y. *Sens. Actuators A* **2014**, *206*, 57.
7. Schmidt, M. In Laser Assisted Net Shape Engineering; Knapp, M.; Clement, S., Franz, C., Eds.; Science: Erlangen, **2010**.
8. Jaeschke, P.; Herzog, D.; Haferkamp, H. *J. Reinf. Plast. Compos.* **2010**, *29*, 3083.
9. Jun, C.; Wei, W.; Yi, Y.; Wei, F.; Yujie, C. *J. Appl. Polym. Sci.* **2010**, *117*, 2964.
10. Lupoi, R.; O'Neill, W. *Surf. Coat. Technol.* **2010**, *205*, 2167.
11. Robitaille, F.; Yandouzi, M.; Hind, S.; Jodoin, B. *Surf. Coat. Technol.* **2009**, *203*, 2954.
12. Robitaille, F.; Yandouzi, M.; Jodoin, B. Thermal Spray: Expanding Thermal Spray Performance to New Markets and Applications; EI: Las Vegas, **2009**.
13. Tapphorn, R. M.; Henness, J. A.; Gabel, H. Thermal Spray: Expanding Thermal Spray Performance to New Markets and Applications; EI: Las Vegas, **2009**.
14. Braun, E.; Levin, B. C. *Fire Mater.* **1987**, *11*, 71.
15. Liu, F. C.; Liao, J.; Nakata, K. *Mater. Des.* **2014**, *54*, 236.
16. Katayama, S.; Kawahito, Y. *Scr. Mater.* **2008**, *59*, 1.
17. Zhequn, H.; Sumio, S.; Jun, Y. J. *Mater. Process. Technol.* **2013**, *214*, 2018.
18. Yu, J.; Hu, S. J.; Guo, J. B.; Min, H.; Qin, S. H. *Eng. Plast. App.* **2010**, *1*, 85.
19. Solid Surface Energy Data (SFE) for Common Polymers. Available at: http://www.kinochina.com/kinochina-Down-16261, **2009**.
20. Yu, Q.; Huang, Y. J.; Yang, Q. *Eng. Plast. App.* **2008**, *06*, 77.
21. Kawahito, Y.; Niwa, Y.; Terajima, T. *Mater. Trans.* **2010**, *51*, 1433.
22. Katayama, S.; Kawahito, Y. *Scripta Mater.* **2008**, *59*, 1247.
23. Ali, N.; Duan, X.; Jiang, Z. T.; Goh, B. M.; Lamb, R.; Tadich, A.; Poinern, G. E. J.; Fawcett, D.; Chapman, P.; Singh, P. *Appl. Surf. Sci.* **2014**, *289*, 560.
24. Sandrin, L.; Sacher, E. *Appl. Surf. Sci.* **1998**, *135*, 339.
25. Tang, D. Y.; Guo, Y. D.; Zhang, X. H.; Liu, J. *Surf. Interface. Anal.* **2009**, *41*, 974.
26. Bébin, P.; Prud'Homme, R. E. *Chem. Mater.* **2003**, *15*, 965.
27. Tan, X. H.; Shan, J. G.; Ren, J. L. *Acta Metall.* **2013**, *06*, 751.